Supplementary Information to "Transmon qubit readout fidelity at the threshold for quantum error correction without a quantum-limited amplifier"

Liangyu Chen[1], Hang-Xi Li[1], Yong Lu[2], Christopher W. Warren[1], Christian J. Križan[1], Sandoko Kosen[1], Marcus Rommel[1], Shahnawaz Ahmed[1], Amr Osman[1], Janka Biznárová[1], Anita Fadavi Roudsari[1], Benjamin Lienhard[3,4], Marco Caputo[5], Kestutis Grigoras[5], Leif Grönberg[5], Joonas Govenius[5], Anton Frisk Kockum[1], Per Delsing[1], Jonas Bylander[1], Giovanna Tancredi[1]

[1]*Department of Microtechnology and Nanoscience, Chalmers University of Technology, 41296 Gothenburg, Sweden.*

[2]*3rd Institute of Physics, University of Stuttgart, 70569 Stuttgart, Germany.*

[3]*Department of Chemistry, Princeton University, Princeton, NJ 08544, USA*

[4]*Department of Electrical and Computer Engineering, Princeton University, Princeton, NJ 08544, USA*

[5]*VTT Technical Research Centre of Finland, FI-02044 VTT, Finland*

(Dated: August 11, 2022)

I. COMMON-MODE PURCELL FILTER

Here, we derive the evolution of the readout resonator-Purcell bandpass filter system with input-output theory [1]. The equations of motion of the classical field amplitudes $\alpha(t)$ and $\beta(t)$ in the readout resonator and in the Purcell filter resonator are, respectively [2],

$$\begin{aligned} \dot{\alpha}(t) &= -i\Delta_{rd}\alpha(t) - iJ\beta(t) - \frac{\gamma_a}{2}\alpha(t), \\ \dot{\beta}(t) &= -i\Delta_{fd}\beta(t) - iJ^*\alpha(t) - \frac{\kappa_f}{2}\beta(t) - i\epsilon_f(t). \end{aligned} \tag{1}$$

Δ_{rd} (Δ_{fd}) $= \omega_{r(f)} - \omega_d$ is the detuning between the resonator frequency ω_r (band-pass center frequency ω_f) and the driving tone at frequency ω_d. J, and its complex conjugate J^*, represent the coupling strength between the readout resonators and the Purcell filter. κ_f is the Purcell filter bandwidth and γ_a is the non-radiative loss rate of the resonator. $\epsilon_f(t)$ is the electric field strength of the driving tone of frequency ω_d, which can be time-dependent for pulsed readout. Note that for simulation, the equations are written in the rotating frame $e^{-i\omega_d t}$ of a monochromatic readout drive frequency, which applies for a continuous readout drive tone. In addition, the three field amplitudes α, β, and ϵ_f are normalized such that $|\alpha|^2$ and $|\beta|^2$ represent the average photon number in the readout resonators and the Purcell filter, respectively. $|\epsilon_f|^2$ is normalized accordingly as well.

We find the steady-state response of the filter on the time scale longer than κ_f^{-1} by solving the equations of motion with the conditions $\dot{\alpha}(t) = 0$ and $\dot{\beta}(t) = 0$. For an ideal resonator, we assume the loss γ_a to be zero to simplify the expression. We find the analytical solution of the steady-state electric field inside the coupled Purcell-resonator system as

$$\beta(\omega_d) = \frac{\Delta_{rd} \cdot \epsilon_f}{(i\Delta_{fd} + \frac{\kappa_f}{2})i\Delta_{rd} + |J|^2}. \tag{2}$$

The transmitted field strength at the output of the Purcell filter is given by $\gamma_{tr} = \beta\kappa_f/2$. We calculate γ_{tr} as a function of the drive frequency ω_d and use it to fit the spectroscopy data and extract the relevant parameters as shown in Supplementary Figure 1.

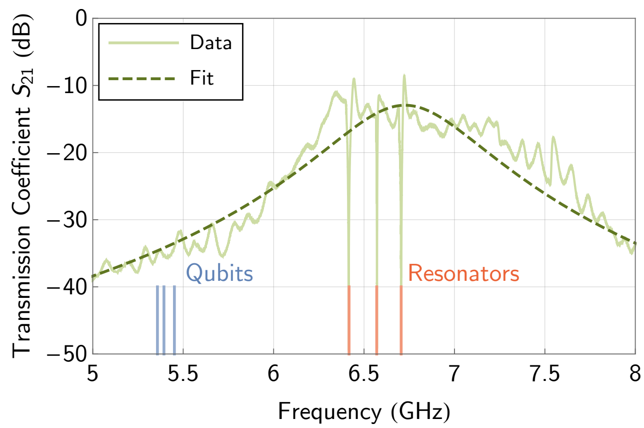

Supplementary Figure 1. **Transmission coefficient S_{21} as a function of the driving frequency ω_d.** The data is shown as the solid line and the fit to Eq. (2) is the dashed line, where the resonator-Purcell coupling J is neglected. The vertical lines indicate the frequencies of the qubits (blue) and the readout resonators (red). The qubits are outside the passband of the Purcell filter and are therefore protected from relaxation into the environment.

To calculate the dynamic response of the field inside the readout resonator, we only assume a quasi-steady state for the Purcell filter, i.e., $\dot{\beta}(t) = 0$, and solve for β in Eq. (1) as a function of $\alpha(t)$,

$$\beta = \frac{-iJ\alpha(t) - i\epsilon_f}{\kappa_f/2 + i\Delta_{fd}}. \tag{3}$$

We then substitute the expression back into the full equation of motion and organize the terms in the following form:

$$\dot{\alpha}(t) = -i(\Delta_{rd} + \delta\omega_r)\alpha(t) - \frac{\kappa_r}{2}\alpha(t) - i\epsilon_r, \tag{4}$$

with an effective linewidth of the readout resonator κ_r, a shift $\delta\omega_r$ of the bare resonator frequency due to the coupling to the Purcell filter, and the effective drive amplitude inside the readout resonator ϵ_r. These parameters are given by

$$\begin{aligned} \kappa_r &= \frac{4|J|^2}{\kappa_f}\frac{1}{1+(2\Delta_{fd}/\kappa_f)^2}, \\ \delta\omega_r &= -\frac{|J|^2{\cdot}\Delta_{fd}}{(\kappa_f/2)^2+\Delta_{fd}^2} = -\frac{\Delta_{fd}}{\kappa_f}\kappa_r, \\ \epsilon_r &= \frac{iJ}{\kappa_f/2+i\Delta_{fd}}\epsilon_f. \end{aligned} \tag{5}$$

Therefore, the qubit excitation decaying through the resonator could be interpreted as driving the resonator at $\omega_d = \omega_q$ with a decay rate

$$\kappa_q = \frac{4|J|^2}{\kappa_f}\frac{1}{1+(2\Delta_{fq}/\kappa_f)^2}, \tag{6}$$

where $\Delta_{fq} = \omega_f - \omega_q$. The qubit Purcell limit on the T_{01} decay is given in [3]

$$\Gamma_{01,\mathrm{Purcell}} \approx \kappa\frac{g^2}{(\omega_r-\omega_q)^2}, \tag{7}$$

With $\kappa = \kappa_q$, we find,

$$\Gamma_{01,\mathrm{Purcell}} \approx \frac{4|J|^2\kappa_f}{\kappa_f^2+4(\omega_f-\omega_q)^2}\frac{g^2}{(\omega_r-\omega_q)^2}. \tag{8}$$

Therefore, $\Gamma_{01,\mathrm{Purcell}}$ can be engineered to be significantly longer than the case with the readout resonator directly coupled to the feedline with a rate κ, while the dispersive shift χ can be sufficiently large to enable fast readout.

Multiple resonators can be coupled within the bandwidth of a single Purcell filter by choosing a corresponding resonance frequency ω_f and linewidth κ_f. Such common designs provide various advantages in scalability compared to dedicating one Purcell filter to each resonator: It reduces the physical footprint on the chip, freeing up space that can instead be used to route control lines to further avoid drive crosstalk. The filter resonator is incorporated into the feedline in a straightforward fashion as a $\lambda/2$ resonator with a capacitor at each end. The fabrication accuracy of the resonator frequencies is less crucial to readout performance since the bandwidth of the Purcell filter κ_f is large, so the filter is insensitive to a small drift in resonator frequency.

One main concern about the common Purcell filter is that the crosstalk between the readout resonators could increase: The measurement could induce phase errors on the untargeted qubits with resonators coupled to the same filter. This effect could be mitigated with pulse schemes to compensate for the phase shift. At the same time, the circuit design should separate qubits into different physical filter lines depending on their designation, e.g., ancilla or data qubit.

II. EXPERIMENTAL SETUP

The parameters of the sample used in our experiment are listed in Supplementary Table I and II. The qubit relaxation time T_{01} is Purcell-limited according to the calculation based on Eq. (7), which is lower than the design value, and what normally achieved in our lab, due to a shift in qubit frequencies during the fabrication process. The device is installed in a Bluefors dilution refrigerator and cooled below 10 mK. The full wiring diagram is shown in Supplementary Figure 2. The drive pulses for the qubits are generated by an 8-channel arbitrary waveform generator (*Zurich Instruments* HDAWG), and are up-converted to the qubit frequency by IQ mixing.

The readout pulse is generated with an ultra-high frequency lock-in amplifier (*Zurich Instruments* QA) and up-converted to the corresponding readout frequency of the individual resonators. The transmitted readout signal through the sample is amplified by around 39 dB at 4 K with a high-electron-mobility transistor (HEMT, LNF-LNA184A) amplifier. Additionally, two amplifiers are connected to the readout chain outside of the dilution fridge. Finally, the output signal is down-converted to the hundreds of MHz range to be recorded and integrated by the QA.

Parameters		R1	R2	R3	PF
Resonator frequency	$\omega_r/2\pi$ (GHz)	6.454	6.606	6.744	6.726
Effective linewidth	κ_r (κ_f) $/2\pi$ (MHz)	16.6	11.0	12.4	820.9
Readout-Purcell coupling	$J/2\pi$ (MHz)	70.1	57.1	60.6	

Supplementary Table I. **Measured resonator parameters for the Purcell filter and the three readout resonators.**

Parameters		Q1	Q2	Q3
Qubit frequency	$\omega_q/2\pi$ (GHz)	5.358	5.395	5.456
Qubit anharmonicity	$\alpha/2\pi$ (MHz)	-192	-198	-199
Qubit-readout coupling	$g/2\pi$ (MHz)	231	235	263
Dispersive shift	$\chi/2\pi$ (MHz)	7.3	6.3	7.0
T_1 Purcell limit	T_P (μs)	2.8	4.5	3.7
Average relaxation time	$\overline{T}_1$ (μs)	3.6	6.2	3.8
Average Ramsey decay time	$\overline{T}_2^*$ (μs)	1.7	1.7	2.0
Average Echo decay time	$\overline{T}_2^e$ (μs)	1.8	2.1	2.2
Thermal population	P_{th}(%)	1.9%	2.0%	1.6%
Single-qubit gate fidelity	$\mathcal{F}_{1Q}$(%)	99.04%	99.59%	99.48%

Supplementary Table II. **Measured qubit parameters, coherence properties, and single-qubit performance for the three qubits.**

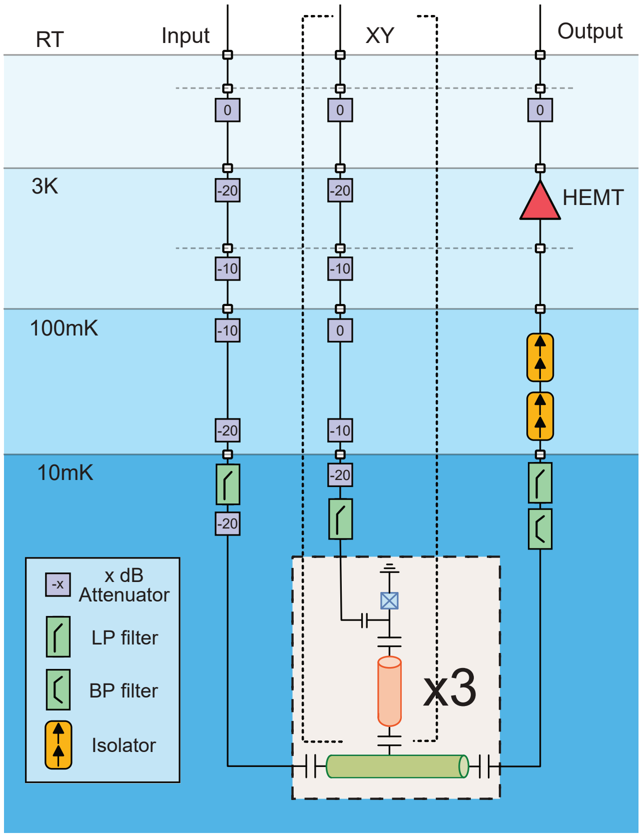

Supplementary Figure 2. **Full wiring diagram for the experimental setup including the circuit model of the tested chip.** LP: low-pass, BP: band-pass, XY: qubit XY-drive line, RT: room temperature.

[1] Gardiner, C. W. & Collett, M. J., Input and output in damped quantum systems: Quantum stochastic differential equations and the master equation, Phys. Rev. A **31**, 3761–3774 (1985).
[2] Sete, E. A., Martinis, J. M. & Korotkov, A. N., Quantum theory of a bandpass Purcell filter for qubit readout, Phys. Rev. A **92**, 012325 (2015).
[3] Blais, A., Huang, R.-S., Wallraff, A., Girvin, S. M. & Schoelkopf, R. J., Cavity quantum electrodynamics for superconducting electrical circuits: An architecture for quantum computation, Phys. Rev. A **69**, 062320 (2004).